A study of conical intersections for the H_3^+ system

P. Barragán, L. F. Errea, A. Macías, L. Méndez, I. Rabadán,* and A. Riera
Departamento de Química, Universidad Autónoma de Madrid, 28049 Madrid, Spain.
Laboratorio Asociado al CIEMAT de Física Atómica y Molecular en Plasmas de Fusión.
(Dated: March 15, 2006)

A parameterization of the three asymptotic conical intersections between the energies of the H_3^+ ground state and the first excited singlet state is presented. The influence of an additional, fourth conical intersection between the first and second excited states at the equilateral geometry on the connection between the three conical regions is studied, for both Diatomics-In-Molecules (DIM) and *ab initio* molecular data.

PACS numbers: 31.50.Gh,31.70.-f,34.20.Mq,34.70.+e

I. INTRODUCTION

In a previous work [1] (I, hence-forward) we presented a comparative study of molecular data for inelastic and reactive collisions involving the H_3^+ quasi-molecule and its isotopical variants. As reviewed in our paper, this system has been the object of many theoretical and experimental works, because of its importance and (apparent) simplicity, of the unique features of molecular energies and non-adiabatic couplings involved, and of the variety of dynamical processes that are at work (see also [2–4]). We shall assume, as in previous work, that at low collision energies only those electronic states of the H_3^+ quasi-molecule asymptotically dissociating into channels $H^+ + H_2(X^1\Sigma_g^+)$, $H(1s) + H_2^+(X^2\Sigma_g^+)$ play a major role, and therefore our interest is focused on the two lowest PESs.

Most dynamical treatments of the $H^+ + H_2$ and $H + H_2^+$ reactions were carried out using the semi-empirical Diatomics-in-Molecules (DIM) method and, in this respect, some of our findings were a little disturbing: while energies and dynamical couplings obtained from *ab initio* calculations did not strongly differ from the corresponding DIM values, this was not so for the residual couplings obtained from a "diabatization" procedure (our quotation marks reflecting the well-known fact that strict diabatic states do not exist for polyatomics). The relevance of this finding lies in that, because of the peculiar features of H_3^+, dynamical treatments usually involve as a first step some kind of diabatization, and residual couplings are neglected. Then, our previous work would seem to invalidate such approaches. However, since it is clear that the quality of the previous treatments reviewed in I cannot be fortuitous, we have analyzed the origin of the problem in more detail.

In our analysis, we found that the main differences in the residual couplings were due to the fact that the integration path that yields the adiabatic-to-diabatic transformation angle crosses values for the extrema of the couplings (at the so-called *loci* in I), which are related to the conical intersections between the first and second adiabatic potential energy surfaces (PES), and that are very sensitive to small variations of the molecular data, and in particular, to how the DIM method is implemented. Another feature that enhances residual couplings along some integration paths is the (unexpected) role of *rotational* (Coriolis) couplings, which are neglected in the standard IOSA and RIOSA approaches [5, 6]. Interestingly, this feature is related to both the above-mentioned conical intersections and to an additional one between the second and third PES in the equilateral nuclear configuration. To complicate things further, this latter intersection apparently differs in the DIM and *ab initio* data.

From all these findings, it is clear that to complete the study of I, a proper understanding of the main features of wave-functions and couplings near the conical intersections between the lowest two PES of the H_3^+ system is needed, and we present here a contribution to this understanding. As we shall see, since the conical regions lie at infinite distances, they do not give rise to geometrical phases [7–9] since nuclear paths do not surround the seams. However, it turns out that the topography of the coupling surfaces is strongly influenced by the geometrical phase of the additional conical seam between the second and third PES – an issue that is related to the so-called linked conical intersections and related topics, which have been well treated in the literature [10–17].

In our present calculations, we used the flexibility of the DIM approach to eliminate unnecessary discrepancies with *ab initio* results. For instance, some numerical differences in the residual couplings obtained in I were due to the use of Morse potentials in the DIM calculations, which caused energy differences of the order of 1 mHartree from the corresponding *ab initio* values. Here, instead of Morse functions, we have used as input for the DIM method our *ab initio* data for the H_2 and H_2^+ energies; therefore, our *ab initio* and new DIM data are extremely close in the relevant asymptotic regions. Another difference with I is that, for the present purposes, we do not perform a diabatization of the molecular states for the whole domain of internuclear distances, since we found that it enhances the effect of unimportant differences between *ab initio* and DIM couplings. In the following section, we replace this by a "regularization"

*Electronic address: Ismanuel.Rabadan@uam.es

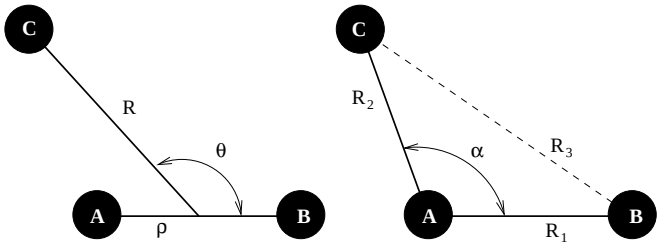

FIG. 1: Jacobi and bond coordinates.

procedure, which is an elimination of quasi-singularities by a local diabatization in the neighborhood of the three seams. Since the DIM and *ab initio* couplings are close there, the procedure can then be employed for both sets of data. In Sec. III we study the connection between the three regularizations, which brings up a link with the fourth seam. Our main conclusions are drawn in Sec. IV.

Atomic units are used throughout.

II. REGULARIZATION

To describe the nuclear configuration of H_3^+ we can employ bond distances and bond angle, Jacobi, or hyperspherical, coordinates. For the purpose of describing, transforming and storing the molecular energies and couplings, it is simpler to limit our consideration to the former two forms. Using an obvious notation (see Fig. 1), a set of Jacobi coordinates and angle is given by $\{\rho, R, \theta\}$, where $\boldsymbol{\rho} = \boldsymbol{R}_{ab}$, $\boldsymbol{R} = \boldsymbol{R}_{ab}/2 + \boldsymbol{R}_{bc}$, $\boldsymbol{R} \cdot \boldsymbol{\rho} = R\rho\cos\theta$; and a set of bond lengths and angle by $\{R_1, R_2, \alpha\}$, with $\boldsymbol{R}_1 = \boldsymbol{R}_{ab}$, $\boldsymbol{R}_2 = \boldsymbol{R}_{ac}$, $\boldsymbol{R}_1 \cdot \boldsymbol{R}_2 = R_1 R_2 \cos\alpha$.

As in I, our *ab initio* data were obtained with a full configuration interaction calculation performed with the program MELD [18]. The molecular orbitals were obtained by means of self consistent field calculations over a basis set of [3s,2p,1d] CGTOs taken from Ref. [19]. The *ab initio* non-adiabatic couplings have been calculated using a numerical derivative technique [20] that has been explained elsewhere [20, 21] and applied to a variety of systems [22, 23]. These couplings are the matrix elements of the nuclear gradient operator $\nabla_{\boldsymbol{R}}$:

$$M_{lm} = \langle \psi_l(\boldsymbol{r};\boldsymbol{R}) | \hat{\boldsymbol{X}} \cdot \nabla_{\boldsymbol{R}} | \psi_m(\boldsymbol{r};\boldsymbol{R}) \rangle \qquad (1)$$

where ψ_i is the i-th molecular state, $\boldsymbol{r}$ are electronic coordinates, $\boldsymbol{R}$ nuclear coordinates and $\hat{\boldsymbol{X}}$ is a unit vector in any direction of $\boldsymbol{R}$-space. Use of bond coordinates then yields the matrix elements $\langle\psi_1|\partial/\partial R_1|\psi_2\rangle$, $\langle\psi_1|\partial/\partial R_2|\psi_2\rangle$ and $\langle\psi_1|\partial/\partial\alpha|\psi_2\rangle$, and use of Jacobi coordinates $\langle\psi_1|\partial/\partial\rho|\psi_2\rangle$, $\langle\psi_1|\partial/\partial R|\psi_2\rangle$ and $\langle\psi_1|\partial/\partial\theta|\psi_2\rangle$.

Our DIM data were obtained as in Ref. [24] and I, except that, as explained in the Introduction, the input data for the H_2 and H_2^+ potential curves were obtained from *ab initio* calculations with the same basis sets as for the H_3^+ quasi-molecule. As an illustration of the agreement between the ensuing $\langle\psi_1|\partial/\partial R_1|\psi_2\rangle$, $\langle\psi_1|\partial/\partial R_2|\psi_2\rangle$ couplings in the neighborhood of a conical intersection, we compare in Fig. 2, as functions of R_1, the data calculated with DIM (full line) and *ab initio* (bullets) methods, for $\alpha = 45°$ and fixed R_2. To illustrate further the shape of these couplings in the conical region, we display their variation with R_2 (for the DIM data only), for fixed R_1, in Fig. 3.

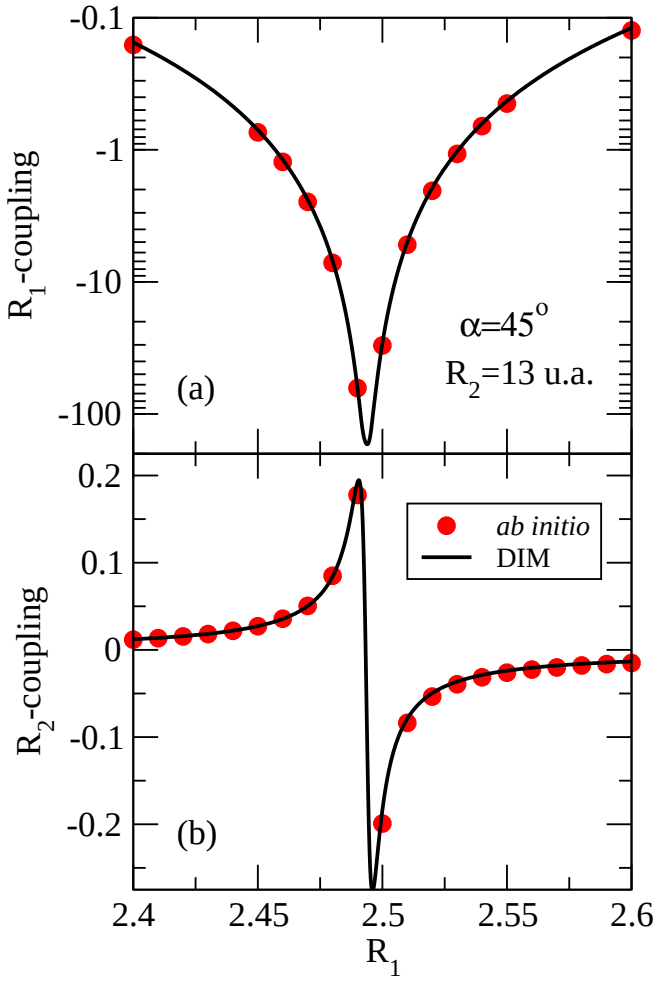

FIG. 2: Cut along R_1 of the two non-adiabatic couplings between the first two singlet states of H_3^+.

As explained in I, the existence of three conical intersections between the two lowest PESs allows to explain an important part of the complicated topography of the non-adiabatic couplings as functions of the nuclear geometry. The intersections arise [3] because the energies of the ground states of the H_2 molecule and the H_2^++H(1s) system accidentally cross for an internuclear distance ρ_0(=2.49226 a_0 in our calculations), see Fig. 4. Hence, in any of the three limits where an internuclear distance, $R_{ab} \equiv R_1$, $R_{ac} \equiv R_2$ or $R_{bc} \equiv R_3$, takes up this value, and the other two tend to infinity, there arises a conical seam between the energies of the ground and first excited state. More precisely, the first seam $R_1 = \rho_0$, and R_2, $R_3 \to \infty$ is a straight line for both coordinate systems

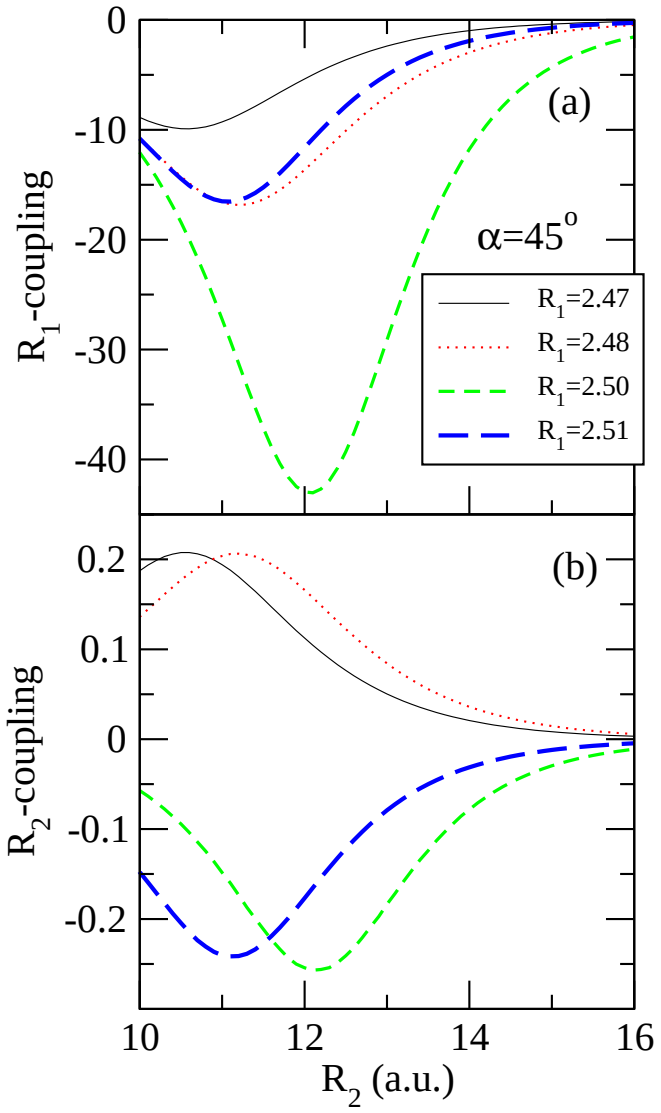

FIG. 3: Several cuts along R_2 of the two non-adiabatic couplings between the first two singlet states of H_3^+.

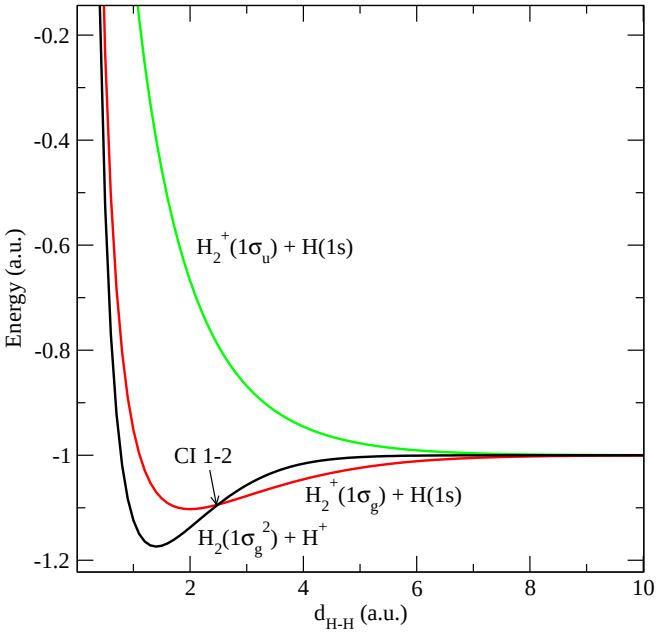

FIG. 4: *Ab initio* diatomic energies used in the DIM calculations.

$\{R_1, R_2, \alpha\}$ and $\{\rho, R, \theta\}$, with $R_1 = \rho_0$ and $\rho = \rho_0$, respectively. The second seam $R_2 = \rho_0$, and R_1, $R_3 \to \infty$ is a straight line in the $\{R_1, R_2, \alpha\}$ system, and an ellipse $R^2 + R\rho\cos\theta + \rho^2/4 = {\rho_0}^2$ in the $\{\rho, R, \theta\}$ system, degenerating into two straight lines $\rho = 2(R \pm \rho_0)$ as $\theta \to \pi$. Finally, the third seam $R_3 = \rho_0$, and R_1, $R_2 \to \infty$ is an ellipse $R_1^2 + R_2^2 - 2R_1R_2\cos\alpha = {\rho_0}^2$ and $R^2 - R\rho\cos\theta + \rho^2/4 = {\rho_0}^2$ for both systems, degenerating into $R_1 = R_2 \pm \rho_0$ and $\rho = 2(R \pm \rho_0)$ in the $\alpha = 0$ and $\theta = 0$ limits, respectively.

As shown e.g. in I, for each conical seam, the "vibrational-type" radial coupling ($\langle\psi_1|\partial/\partial R_1|\psi_2\rangle$ or $\langle\psi_1|\partial/\partial\rho|\psi_2\rangle$ for the first seam), as a function of R_1, or ρ (for the same seam), tends to a delta function in the asymptotic limit where the "translational" coordinate (R_2 or R) tends to infinity, and the "translational-type" coupling ($\langle\psi_1|\partial/\partial R_2|\psi_2\rangle$ or $\langle\psi_1|\partial/\partial R|\psi_2\rangle$) abruptly changes sign (see e.g. Figs. 2a and 3b). Our regularization consists of eliminating these quasi-singular behaviors by a local diabatization procedure, obtained from an analytical fit of the molecular data. The procedure applies to the three seams, because the couplings in the second and third seams are obtained, up to a sign, by interchanges of the coordinates $R_1 \leftrightarrow R_2$ and $R_1 \leftrightarrow R_3$ from the data for the first seam. The origin of the relative sign is analyzed in the following section.

To perform the diabatization, we employed (see I) a linear model [25, 26] for the diabatic energy difference $\Delta H(R_1) \equiv H_{22} - H_{11}$ as a function of the "vibrational" coordinate R_1, or ρ, together with an exponentially decreasing interaction $H_{12}(R_2)$ between the diabatic states, as a function of the "translational" coordinate R_2, or R. We then used this linear-exponential model to obtain the adiabatic-to-diabatic transformation angle from the standard expression:

$$\tan 2\xi = \frac{2H_{12}}{H_{22} - H_{11}} \tag{2}$$

with

$$H_{22} - H_{11} = d(R_1 - R_0) \tag{3}$$

$$H_{12} = k(1 + R_2)e^{-R_2} \tag{4}$$

where the seam is located at $R_1 = R_0$, which is very close to ρ_0, so that to accurately fit the couplings, it is sufficient to allow for a small R_2-dependence of R_0:

$$R_0 = \rho_0 + Be^{-0.285R_2} \tag{5}$$

Then, the transformation angle is given by:

$$\tan 2\xi = \frac{2k(1 + R_2)e^{-R_2}}{d(R_1 - R_0)} \tag{6}$$

which leads to the parameterized expressions for the non-adiabatic couplings:

$$\frac{\partial \xi}{\partial R_1} = -\frac{0.5\delta}{(R_1 - R_0)^2 + \delta^2} \tag{7}$$

and

$$\frac{\partial \xi}{\partial R_2} = \frac{0.5\delta}{(R_1 - R_0)^2 + \delta^2} \left(0.285(\rho_0 - R_0) - \frac{R_2(R_1 - R_0)}{1 + R_2} \right) \tag{8}$$

with

$$\delta = \frac{2k}{d}(1 + R_2)e^{-R_2} \tag{9}$$

By fitting the $\langle \psi_1 | \partial / \partial R_1 | \psi_2 \rangle$ coupling to the analytical expression (7), we obtained the values of the parameters δ and R_0. This was done for $R_1 \in [2.45, 2.55]$ at several values of $R_2 \in [10, 15]$; the variance of this fit $\bar{\sigma^2}$ varies from 1×10^{-5} for $R_2 = 10$ to 1×10^{-11} for $R_2 = 15$. These values of δ and R_0 were then fitted as functions of R_2 according to Eqs. (5) and (9) for values of $R_2 \in [12, 14]$ and for each value of α considered; in this case, σ^2 is of the order of 1×10^{-10} for both R_0 and δ. Because of the computational efficiency of the DIM approach, this procedure was carried out for the DIM couplings. In Fig. 5 we show the accuracy of the fit by comparing the curves obtained from the analytical expression to the DIM values. To show that our regularization can also be used for the corresponding *ab initio* data (to be employed for instance to extrapolate them), we also include these results in the figure.

As a next step to achieve an overall fit, we then consider the angular variation of the parameters B and $2k/d$, using Eqs. (10) and (11) below. This procedure yields an adjustment with variances $\bar{\sigma^2}$ that are 4.8 and 6.7×10^{-8} for $2k/d$ and B, respectively.

$$2k/d = 152.716e^{-3.7653 \times 10^{-4}\alpha^2} + 16.8855 \tag{10}$$

$$B = 0.036224e^{-1.723 \times 10^{-4}\alpha^2} + 0.0351827 \tag{11}$$

These angular variations are displayed in Fig. 6 (α in degrees).

From our fit, the regularization of the first conical region follows the usual procedure. Use of the transformation $\phi_1 = \cos\xi\ \psi_1 - \sin\xi\ \psi_2, \phi_2 = \sin\xi\ \psi_1 + \cos\xi\ \psi_2$ from adiabatic $\{\psi_1, \psi_2\}$ to diabatic $\{\phi_1, \phi_2\}$ wave functions in the neighborhood of the first seam yields ΔH of Eq. (3) and H_{12} of Eq. (4), together with residual "regularized" couplings $\langle \psi_1 | \partial / \partial R_1 | \psi_2 \rangle - \partial \xi / \partial R_1$ and $\langle \psi_1 | \partial / \partial R_2 | \psi_2 \rangle - \partial \xi / \partial R_2$, which are, as expected, without singularities. As an illustration, we show in Figs. 7 and 8 contour plots of the non-adiabatic (a) and residual (b) couplings: we see that the latter are negligible in the first conical domain. Although for clarity we display these data in a wider region, in practice the regularization should be restricted to this local domain by means of an appropriate cut-off function, depending on applications.

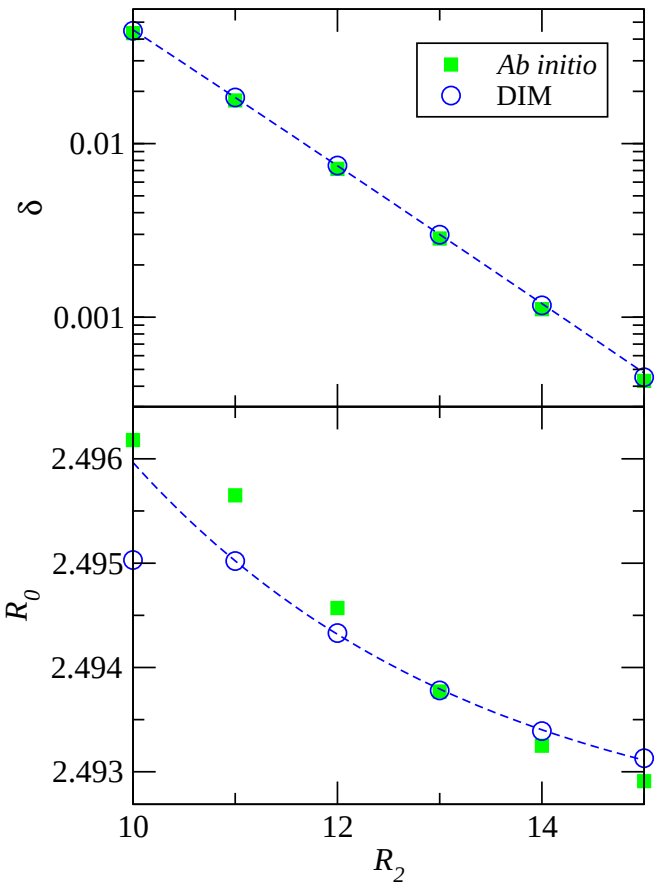

FIG. 5: δ and R_0 parameters obtained from the fit of Eq. (7) to the DIM data at several values of R_2. *Ab initio* results are also given for comparison purposes. The lines are the result of fitting the functionals (5) and (9) to fitted parameters δ and R_0. This results correspond to $\alpha = 45^\circ$.

The regularization of the second conical domain is obtained by interchanging $R_1 \leftrightarrow R_2$ in the previous equations, and changing the sign of ξ should the couplings have opposite signs in the first and second domains. This yields a transformation angle ξ'. Finally, the third domain is regularized by the transformation angle ξ'' obtained by interchanging $R_1 \leftrightarrow R_3$, and changing sign if appropriate. In this way, we are able to perform local regularizations of the non-adiabatic couplings in the three conical regions. However, these procedures cannot be carried out independently, because the sign of the couplings in the three domains are not independent, as we show in the next section, where the connection between the couplings at the three regions is discussed.

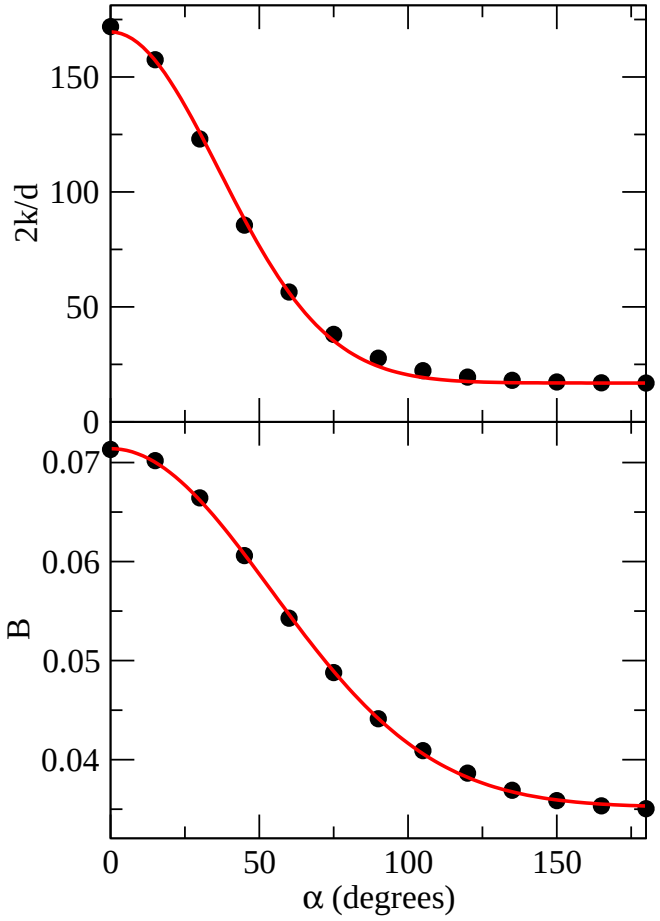

FIG. 6: Symbols: the values of $2k/d$ and B at several values of α. Lines: Eqs. (10) and (11).

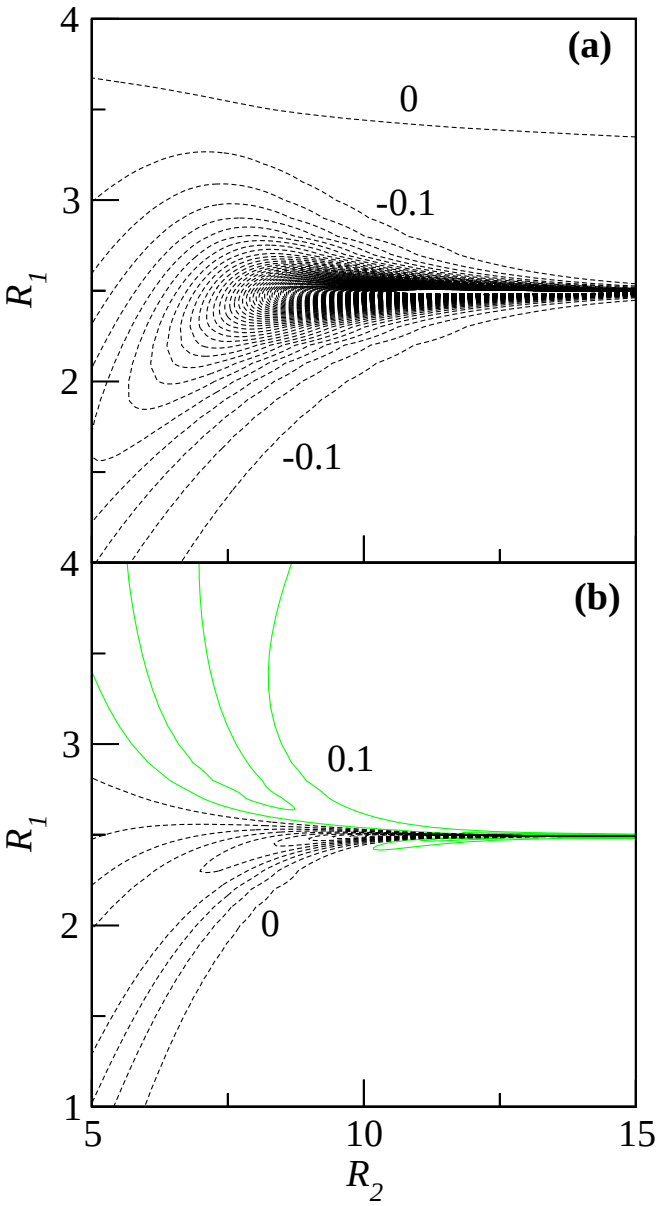

FIG. 7: Contour lines of (a) $\langle\psi_1|\partial/\partial R_1|\psi_2\rangle$ and (b) $\langle\psi_1|\partial/\partial R_1|\psi_2\rangle - \partial\xi/\partial R_1$, residual left by the 3D model in a region of $\{R_1, R_2\}$ for $\alpha = 45^\circ$. Solid lines correspond to positive values and dashed lines are negative values. Starting from 0 (marked in the plot), the levels are separated in steps of 0.1 a_0.

III. CONNECTION BETWEEN THE THREE CONICAL DOMAINS.

A. Topography of the couplings.

We display in Figs. 9 and 10 contour plots of $\langle\psi_1|\partial/\partial R_1|\psi_2\rangle$ and $\langle\psi_1|\partial/\partial R_2|\psi_2\rangle$, respectively, in the $\{R_1, R_2\}$ plane, for $\alpha \approx 0$ (a), $\pi/4$ (b) and $\pi/2$ (c). Plots for angles $0 < \alpha < \pi/3$ and $\pi/3 < \alpha < \pi$ are very similar to Figs. 9b, 10b and 9c, 10c, while for $\alpha \approx 0$ the situation is similar to Figs. 9a, 10a.

The topography of the present surfaces is a little simpler than that of the $\langle\psi_1|\partial/\partial\rho|\psi_2\rangle$, $\langle\psi_1|\partial/\partial R|\psi_2\rangle$ couplings, presented in I, and follows from the explanation given in the previous section. In each figure, we have two conical limit points $R_1 = R_0$, $R_2 \to \infty$ and $R_2 = R_0$, $R_1 \to \infty$, which arise from the intersection of the first two conical seams with the planes $\alpha = 0, \pi/4$ and $\pi/2$, respectively. In addition, for $\alpha \approx 0$, we have a pair of extra limit points corresponding to the third seam considered in the previous section (ellipse degenerating into the straight lines $R_3 = R_0, R_1 = R_2 \pm R_0 \to \infty$). Some additional features are unrelated to the conical seams, such as the relative extrema of the couplings along the straight lines $R_1 = R_2$ (for $\alpha > \pi/3$), or $R_1 = R_3$ and $R_2 = R_3$ (for $\alpha < \pi/3$). As commented in I, these are due to a triple avoided crossing of the lowest PESs for nuclear geometries such that they become quasi-degenerate. To accurately describe the dynamics taking place in these domains of nuclear configurations, a two-state representation is probably insufficient. Here we focus on the neighborhood of the conical points, where the two-state representation is accurate.

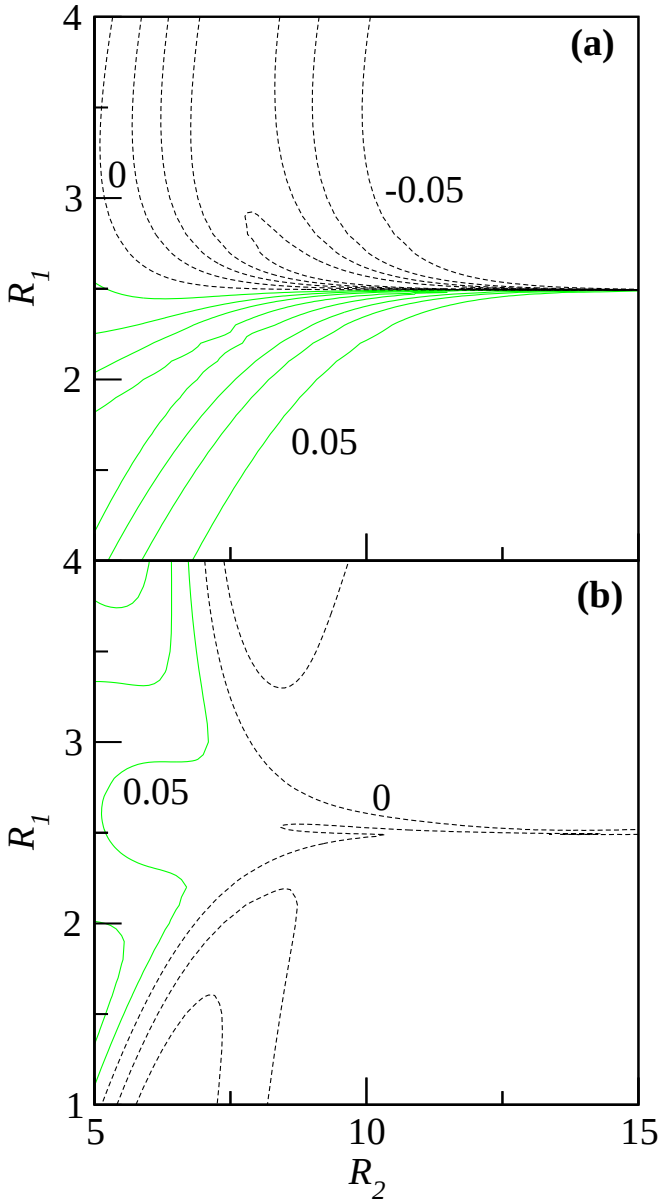

FIG. 8: Same a in Fig. 7 but for $\langle\psi_1|\partial/\partial R_2|\psi_2\rangle$. Levels are separated in steps of 0.05 a_0.

Starting with the first conical domain, the shape of the couplings is straightforwardly explained from the fitting procedure of the previous section, which we can now simplify by neglecting the R_0 dependence on R_2. The most conspicuous features correspond to the R_1 variation of $\langle\psi_1|\partial/\partial R_1|\psi_2\rangle$ and the R_2 variation of $\langle\psi_1|\partial/\partial R_2|\psi_2\rangle$. The former is given by $\partial\xi/\partial R_1$ in Eq. (7) and, as a function of R_1, is a negative Lorentzian peak of height $(2\delta)^{-1}$ and width δ (as in Fig. 2a) that tends to a delta function in the limit $R_2 \to \infty$ (so that $\delta \to 0$, see Eq. (7)). The latter is given by $\partial\xi/\partial R_2$ in Eq. (8), and, as a function of R_2, is a Demkov-type interaction with a roughly constant maximum that shifts to infinity and then changes sign as R_2 crosses R_0 (see fig 3b); as a function of R_1, it

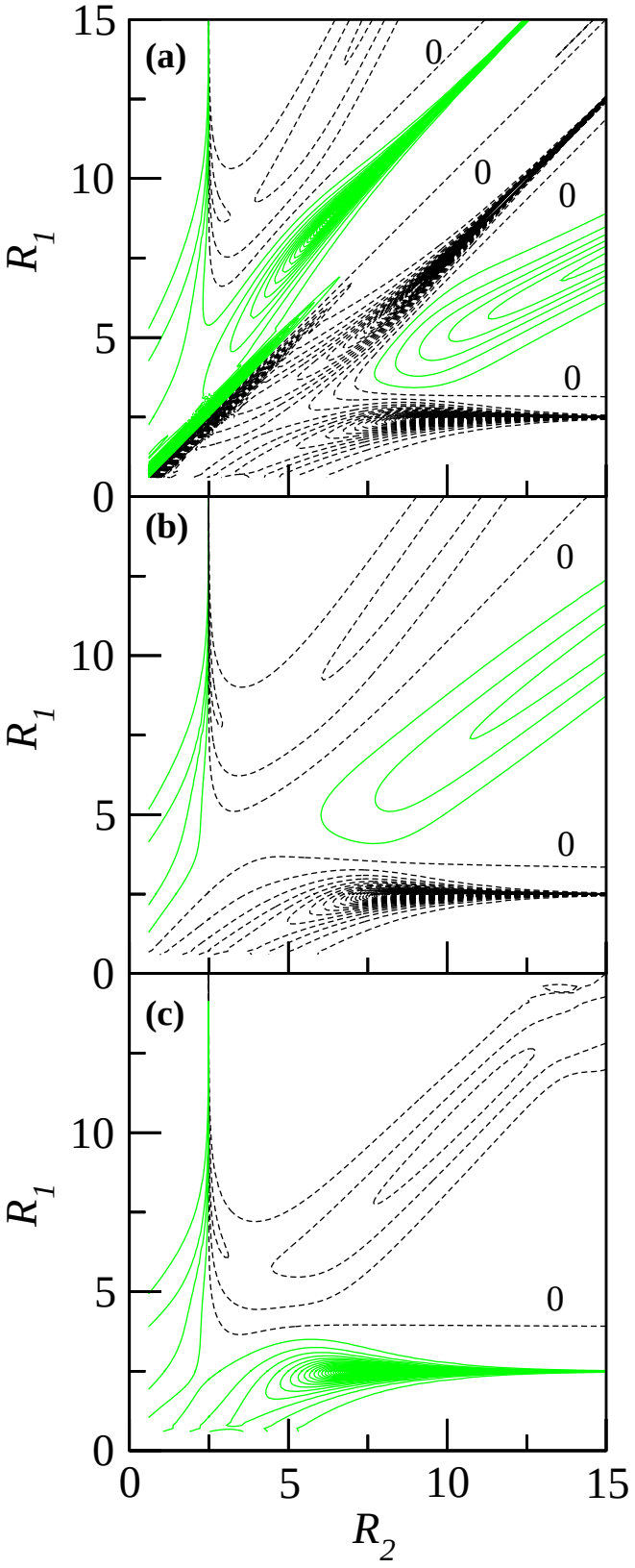

FIG. 9: Contour plot of $\langle\psi_1|\partial/\partial R_1|\psi_2\rangle$ for (a) $\alpha \approx 0$, (b) $\alpha = \pi/4$ and (c) $\alpha = \pi/2$. Solid lines correspond to positive values and dashed lines are negative values. Starting from 0 (marked in the plot), the levels are separated in steps of 0.1 a_0.

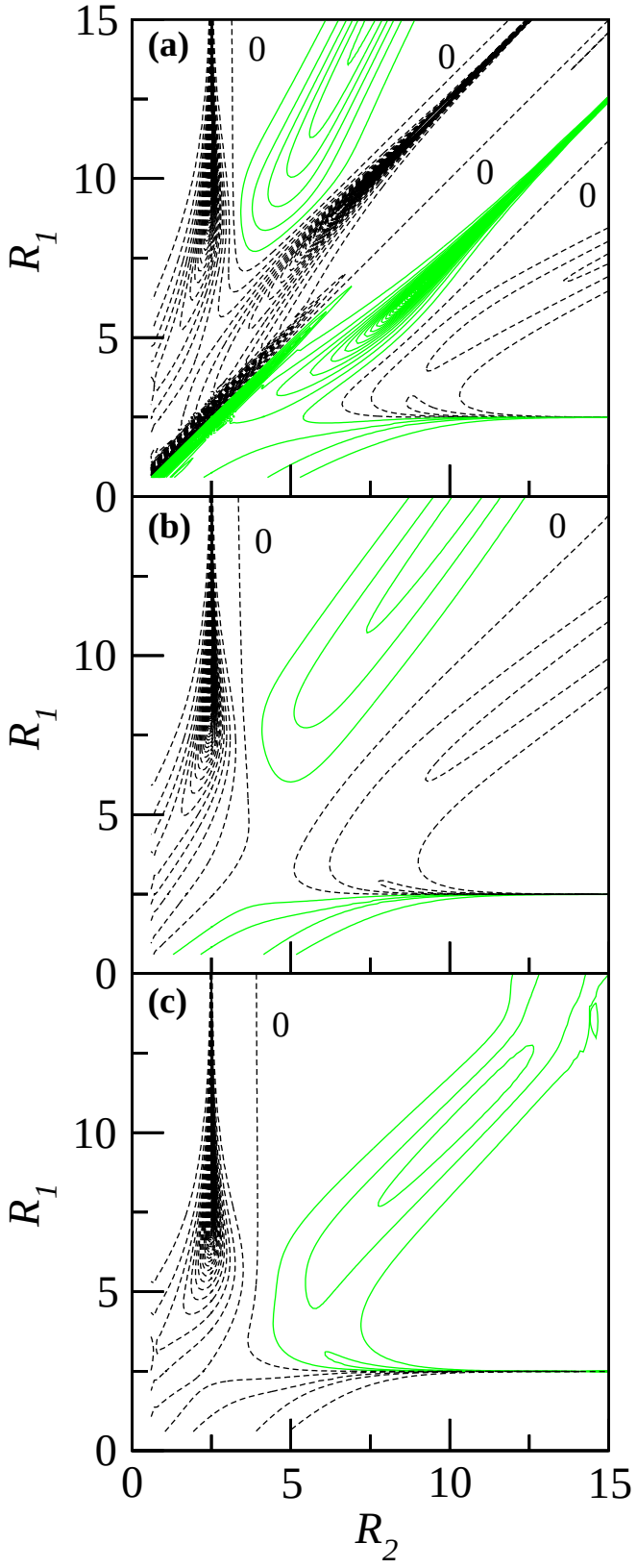

FIG. 10: Same as Fig. 9 but for $\langle\psi_1|\partial/\partial R_2|\psi_2\rangle$.

displays a double peak as in Fig. 2b.

Next, we can understand the shape of $|\langle\psi_1|\partial/\partial R_1|\psi_2\rangle|$, in the second conical region $R_2 \approx R_0$, R_1 large, and according to the reasoning at the end of the previous section, by considering $\partial\xi'/\partial R_1$, which is obtained from $\partial\xi/\partial R_2$ by interchanging $R_1 \leftrightarrow R_2$. Similar reasonings can be applied to $|\langle\psi_1|\partial/\partial R_2|\psi_2\rangle|$ in the second domain.

In addition to those features, the drawings of $\langle\psi_1|\partial/\partial R_1|\psi_2\rangle$ for $\alpha \approx 0$ (Fig. 9a) display two extra Lorentzian peaks for $R_1 \approx R_2 \pm R_0$. These are due to the third conical seam $R_3 = R_0$ in the limit $R_1, R_2 \to \infty$. In its neighborhood, $\langle\psi_1|\partial/\partial R_3|\psi_2\rangle \approx \partial\xi''/\partial R_3$ for R_2 fixed (see previous section), which is obtained from Eq. (7) by interchanging $R_1 \leftrightarrow R_3$. A straightforward use of the chain rule then yields for the matrix element obtained by keeping R_1 fixed $\langle\psi_1|\partial/\partial R_2|\psi_2\rangle \approx \pm\partial\xi''/\partial R_3 + \partial\xi''/\partial R_2$, where the Lorentzian peak of the first term dominates the second term.

We now come to the question of the relative *sign* of the couplings. From the symmetry of the H_3^+ quasi-molecule, we have seen that in Fig. 10a,b,c, the values of $|\langle\psi_1|\partial/\partial R_2|\psi_2\rangle|$ in the first conical region can be readily obtained from $|\langle\psi_1|\partial/\partial R_1|\psi_2\rangle|$ in the second region (Figs. 9a,b,c), by interchanging $R_1 \leftrightarrow R_2$. On the other hand, this symmetry does not tell us anything about the relative sign of the couplings, which is not arbitrary, and stems from both continuity of each coupling in going from one to the other region, and from the relative sign of the two couplings in a given region. In turn, the latter follows from (2) for the transformation angle, under quite general assumptions for ΔH and H_{12} which do not depend on our particular fit.

First, since $\Delta H(R_1)$ vanishes at R_0, we must have:

$$\mathrm{sign}\left(\Delta H \frac{d\Delta H}{dR_1}\right) = \mathrm{sign}(R_1 - R_0) \qquad (12)$$

and from the exponentially decreasing character of $H_{12}(R_2)$:

$$\mathrm{sign}\left(H_{12}\frac{dH_{12}}{dR_2}\right) < 0 \qquad (13)$$

Then, from Eq. (2):

$$\begin{aligned}\mathrm{sign}\left(\frac{\partial\xi}{\partial R_1}\frac{\partial\xi}{\partial R_2}\right) &= -\mathrm{sign}\left(\Delta H\frac{d\Delta H}{dR_1}H_{12}\frac{dH_{12}}{dR_2}\right)\\ &= \mathrm{sign}(R_1 - R_0) \qquad (14)\end{aligned}$$

This unambiguously sets the relative sign of the couplings: $\partial\xi/\partial R_2$ has the same sign as $\partial\xi/\partial R_1$ for $R_1 > R_0$ and the opposite sign for $R_1 < R_0$. Turning now to Fig. 10b, we see that for $\alpha < \pi/3$ the $\langle\psi_1|\partial/\partial R_1|\psi_2\rangle$ coupling is given by the mirror image of $\langle\psi_1|\partial/\partial R_2|\psi_2\rangle$ by interchanging $R_1 \leftrightarrow R_2$, while in Fig. 10c for $\alpha > \pi/3$ we must take the opposite of the mirror image. Since the electronic configurations obtained when interchanging $R_1 \leftrightarrow R_2$ are the same, we conclude that there must be a sign reversal in continuously following a path from

a conical region to the other. We shall now see that the problem is due to the fact that for the equilateral configuration $R_1 = R_2 = R_3$ at $\alpha = \pi/3$ the first and second excited states transform like a two-dimensional E' representation of the D_{3h} point group, so that their energies become degenerate, and this extra conical intersection has a geometrical phase ascribed to it.

Now, since the pioneer work of Ref. [7], the subject of geometrical phases has drawn a large amount of attention. For molecular systems, the standard way to identify the phase is by integrating the coupling M_{23} (not considered here) along a small enough path Γ enclosing the fourth seam such that a two-state model is accurate. As an illustration, we choose the loop in bond coordinates $\{R_1, R_2, \alpha\}$ defined by

$$\Gamma(\beta) = (5 - 0.2\cos\beta, 5 + 0.2\cos\beta, \frac{\pi}{50}\sin\beta + \frac{\pi}{3}) \quad (15)$$

with $\beta \in [0, 2\pi]$, to integrate

$$\gamma_{23}(\beta) = \int_\Gamma M_{23} d\ell = \int_0^\beta \langle\psi_2(\boldsymbol{r};\boldsymbol{R})|\partial/\partial\beta'|\psi_3(\boldsymbol{r};\boldsymbol{R})\rangle d\beta' \quad (16)$$

and the geometrical phase $\gamma_{23}(2\pi)$ reaches a value of π [11, 27, 28], as shown in Fig. 11, which displays the values of the two molecular energies, the non-adiabatic coupling and the phase $\gamma_{23}(\beta)$ along the path. Hence, although the three conical seams we are dealing with here are at infinity, and have therefore no geometrical phase ascribed to them individually, the relative sign of the wave functions are determined by the geometrical phase due to a fourth conical intersection at finite distances. Since the change of sign affects the wave functions of the second, and not of the first, state, it also affects the couplings between them: both $\langle\psi_1|\partial/\partial R_1|\psi_2\rangle$ and $\langle\psi_1|\partial/\partial R_2|\psi_2\rangle$ are discontinuous, as functions of α, which may be seen from superposing Figs. 9b and 9c: while the values in the second conical region qualitatively coincide, they have opposite signs in the first domain. Then, when setting up the interpolation grid to treat the dynamics, even after regularizing the asymptotic domain, we have that the discontinuity persists at smaller distances. What is disturbing, however, is that no sign problem appeared for the $\langle\psi_1|\partial/\partial\rho|\psi_2\rangle$ and $\langle\psi_1|\partial/\partial R|\psi_2\rangle$ couplings in I. Hence, we have investigated the matter further, using the relation between wave function evolution and non-adiabatic couplings [29]. The advantage of such an approach, which is summarized in the next section, is that allows to systematically describe the structure of the wave functions for the lowest two states of interest here in bond or Jacobi parameter space.

B. Electronic structure in terms of bond coordinates

To describe this structure, we choose paths in nuclear configuration space for such large distances that resonance forces dominate and the wave functions take a particularly simple valence-bond form. Though this is inspired by the pioneer approach of Herzberg and Longuet-Higgins [7, 9], our discussion will not be a repetition of that explanation for H_3, where covalent bonds and the antisymmetric character of the wave functions were essential. The loops, qualitatively shown in Fig. 12, surround the conical seam between the second and third PES in the equilateral triangle configuration $R_1 = R_2 = R_3, \alpha = \pi/3$.

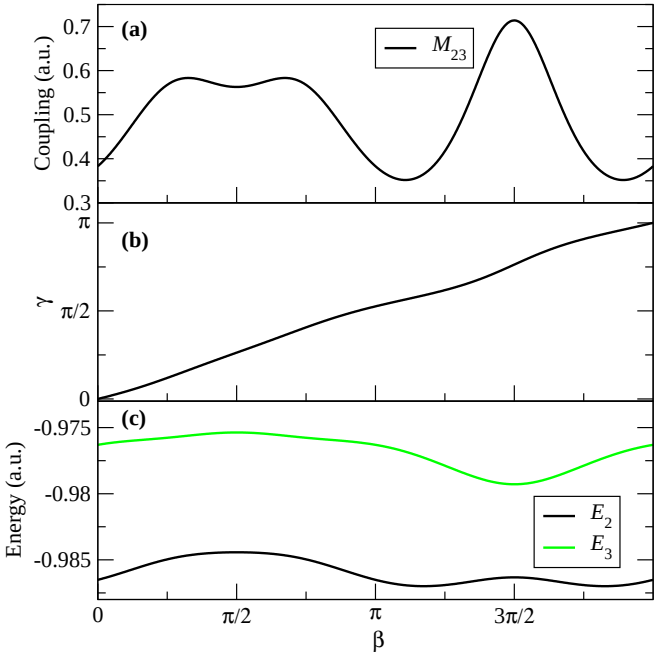

FIG. 11: For the path Γ defined by Eq. (15), the panels show: (a) $M_{23}(\beta)$; (b) $\gamma_{23}(\beta)$ (see Eq. (16)); (c) the energies of the second a third states of H_3^+.

In table I we (qualitatively) display the sequence of dominant valence-bond-type configurations making up ψ_1 and ψ_2, at the reference points marked in Figs. 12 and 13. As an illustration, we plot in Fig. 14 the non-adiabatic couplings $\langle\psi_1|\partial/\partial R_1|\psi_2\rangle$ and $\langle\psi_1|\partial/\partial R_2|\psi_2\rangle$, and the energies of the first and second state of H_3^+, along a path of the type illustrated in Fig. 12, defined by straight line segments joining the points (R1,R2) = (0.5,10), (10,10) and (10,0.5) for $\alpha = \pi/4$, and (10,0.5), (10,10) and (0.5,10) for $\alpha = \pi/2$.

The reference points in Figs. 12 and 13 are chosen such that they either represent a definite nuclear configuration, like AB+C, or that crossing them causes a qualitative change in the electronic structures – for instance, many correspond to a nuclear configuration where a pair of two-body interactions (A-B, B-C or A-C) are the same. For the sake of conciseness, the (singlet) spin part of the wave functions is omitted, and they are not antisymmetrized. Point 1 corresponds to the situation $\alpha < \pi/3$, $R_1 < R_0$, R_2 large, where the nuclear configuration is AB+C, and the configurations of lowest energy represent H_2+H^+ and $H_2^+(\sigma_g)$+H, respectively. The asymp-

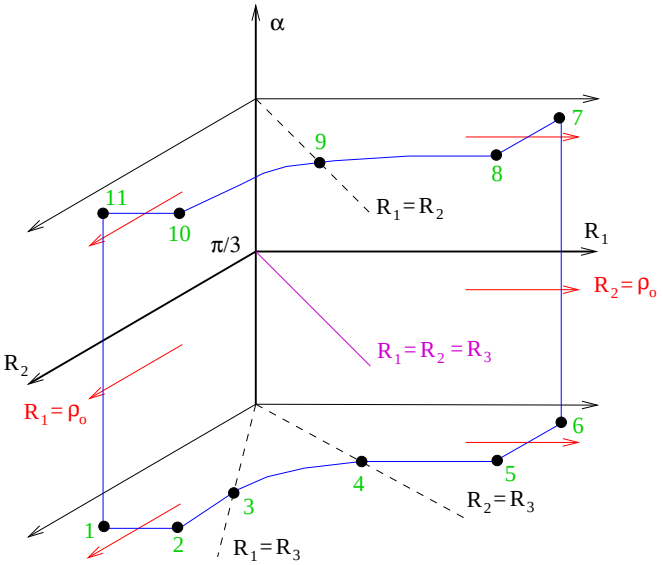

FIG. 12: Cycle in configuration space around the conical seam for $R_1 = R_2 = R_3$; $\alpha = \pi/3$, in bond coordinates.

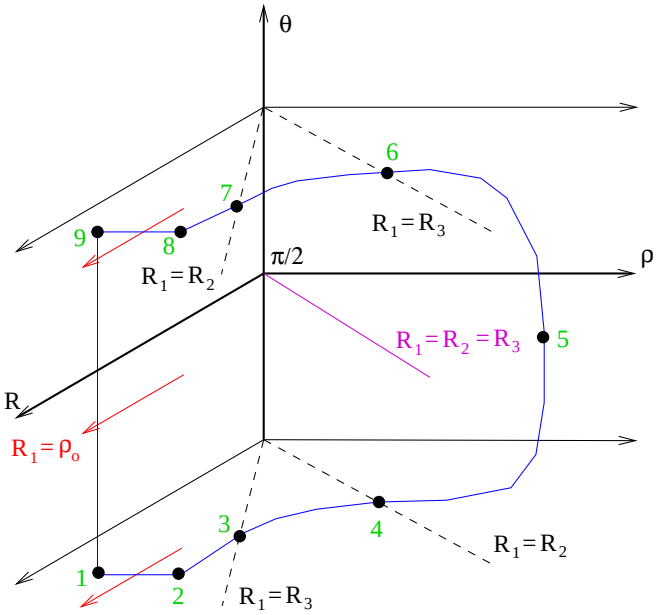

FIG. 13: Cycle in configuration space around the conical seam for $\rho = R_1 = R_2 = R_3 = 2R/\sqrt{3}; \theta = \pi/2$, in Jacobi coordinates.

totic conical point between the energies of the lowest two states appears for $R_2 \to \infty$ and for the value of $R_1 = \rho_0$, where the energies of H_2 and H_2^++H cross. For R_2 finite, the PES avoid crossing at a value $R_1 = R_0$ (see previous section) and we accordingly have a peak of the $\partial/\partial R_1$ coupling there (Eq. (7) and Fig. 2). This *locus* of the coupling is indicated with an arrow in the figure. We cross this *locus* when going from point 1 to point 2, and, as befits a pseudo-crossing, the character of ψ_1 and ψ_2 are interchanged, with one sign reversal.

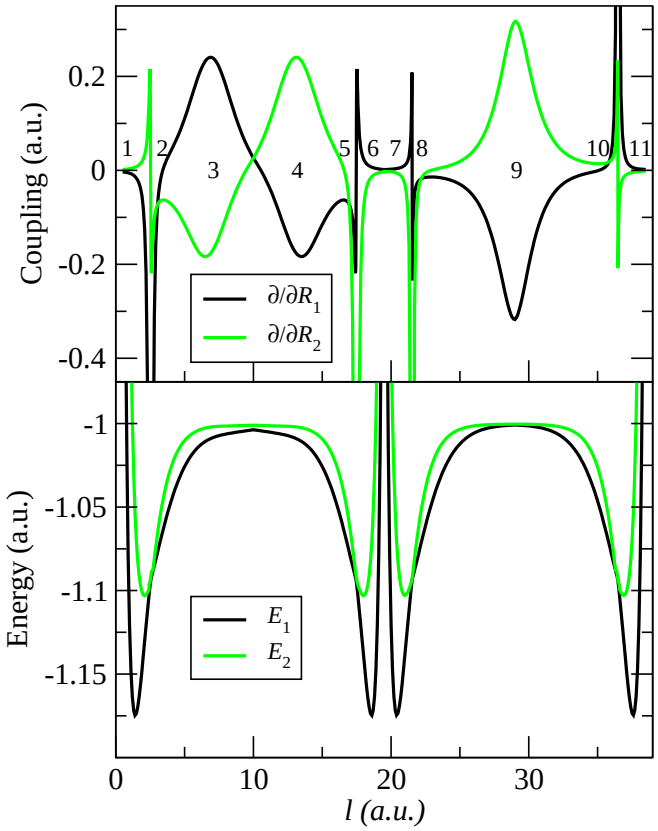

FIG. 14: Non-adiabatic couplings $\langle\psi_1|\partial/\partial R_1|\psi_2\rangle$ and $\langle\psi_1|\partial/\partial R_2|\psi_2\rangle$ (top panel) and energies (bottom panel) in a cycle similar to that of Fig. 12 defined by straight line segments joining the points (R1,R2) = (0.5,10), (10,10) and (10,0.5) for $\alpha = \pi/4$, and (10,0.5), (10,10) and (0.5,10) for $\alpha = \pi/2$ The numbers in the figure approximatively indicate the positions of the reference points of Fig. 12.

Following the path of Fig. 12, we then reach point 3, where $R_1 = R_3 < R_2$, so that the A-B and B-C resonance forces are of the same strength. As mentioned in the previous section and in I, we have a triple pseudo-crossing situation; the ψ_1 and ψ_2 wave functions then take up a bonding and anti-bonding character, respectively, along the R_2 axis. Then, following along the path from a little before to a little after point 3, the wave functions are related by an $s_a \leftrightarrow s_c$ interchange together with sign reversal for ψ_2. A similar situation is encountered as one crosses point 4, where $R_2 = R_3 < R_1$ and the A-C and B-C interactions are of the same strength. Crossing this point leads to an $s_b \leftrightarrow s_a$ interchange together with sign reversal for the second state. In total, going from point 2 to point 5 we have an $s_b \leftrightarrow s_c$ interchange with no sign change. Next, going from step 5 to 6 is the same as from 2 to 1, by exchanging R_1 and R_2 (i.e., B and C). We end up at reference point 6 with the nuclear configuration AC+B.

From this point onwards, the simplest way to proceed is to stop following the cycle, and re-start our walk at the other end AB+C, points 11 and 10, where the situation

TABLE I: Dominant valence-bond character at the reference points marked in Figs. 12 and 13.

	Bond coord.		Jacobi coord.	
Reference point	ψ_1	ψ_2	ψ_1	ψ_2
1	$-s_a s_b$	$\frac{1}{\sqrt{2}}(s_a+s_b)s_c$	$-s_a s_b$	$\frac{1}{\sqrt{2}}(s_a+s_b)s_c$
2	$\frac{1}{\sqrt{2}}(s_a+s_b)s_c$	$s_a s_b$	$\frac{1}{\sqrt{2}}(s_a+s_b)s_c$	$s_a s_b$
3	$\frac{1}{2}(s_a+s_c)s_b+\frac{1}{\sqrt{2}}s_a s_c$	$\frac{1}{\sqrt{2}}(s_a-s_c)s_b$	$\frac{1}{2}(s_a+s_c)s_b+\frac{1}{\sqrt{2}}s_a s_c$	$\frac{1}{\sqrt{2}}(s_a-s_c)s_b$
4	$\frac{1}{2}(s_a+s_b)s_c+\frac{1}{\sqrt{2}}s_a s_b$	$\frac{1}{\sqrt{2}}(s_a-s_b)s_c$	$\frac{1}{\sqrt{2}}(s_b+s_c)s_a$	$-s_b s_c$
5	$\frac{1}{\sqrt{2}}(s_a+s_c)s_b$	$s_a s_c$	$\frac{1}{2}(s_a+s_b)s_c+\frac{1}{\sqrt{2}}s_a s_b$	$\frac{1}{\sqrt{2}}(s_a-s_b)s_c$
6	$-s_a s_c$	$\frac{1}{\sqrt{2}}(s_a+s_c)s_b$	$\frac{1}{\sqrt{2}}(s_a+s_c)s_b$	$-s_a s_c$
7	$-s_a s_c$	$-\frac{1}{\sqrt{2}}(s_a+s_c)s_b$	$\frac{1}{2}(s_b+s_c)s_a+\frac{1}{\sqrt{2}}s_b s_c$	$\frac{1}{\sqrt{2}}(s_b-s_c)s_a$
8	$\frac{1}{\sqrt{2}}(s_a+s_c)s_b$	$-s_a s_c$	$\frac{1}{\sqrt{2}}(s_a+s_b)s_c$	$s_a s_b$
9	$\frac{1}{2}(s_b+s_c)s_a+\frac{1}{\sqrt{2}}s_b s_c$	$\frac{1}{\sqrt{2}}(s_b-s_c)s_a$	$-s_a s_b$	$\frac{1}{\sqrt{2}}(s_a+s_b)s_c$
10	$\frac{1}{\sqrt{2}}(s_a+s_b)s_c$	$s_a s_b$		
11	$-s_a s_b$	$\frac{1}{\sqrt{2}}(s_a+s_b)s_c$		

is identical to points 1 and 2, save that now $\alpha > \pi/3$, so that the A-B and A-C interactions are always larger than the B-C one. We then have an isosceles configuration (point 9) where $R_1 = R_2$ and the A-C and A-B interactions are the same, and, when crossing this point, we have an interchange $s_b \leftrightarrow s_c$ with sign reversal for the second state. We thus reach point 8 with the same configurations as in point 5 but with a sign reversal for the second state; hence, the radial couplings between the two states have opposite signs for $\alpha < \pi/3$ (point 5) and $\alpha > \pi/3$ (point 8), and a consequence is that it is now the ground (and not the excited) state that changes sign and takes up the character of the latter when crossing the arrow (*locus*). We end up (point 7) with ψ_2 having the opposite sign as would be found when following the path from point 6.

We can now consider going around a full cycle, starting from point 6 to points 1 and 11, and then to points 9, 8, 7. Along this loop, we have 7 sign reversals in total, and we end up with an overall sign change for the second state. If we choose to follow numerical order, and start from point 1 following the loop to point 11, continuity then entails to change the sign of the second wave function at points 7 to 11 from those of Table I. We then end up at point 11 with the opposite sign of point 1. Similarly, if we choose to go around the smaller loop 2-5-8-10 we have 3 sign reversals – hence, still an overall sign change, as one expects from the topological reasonings of Ref. [9]. The practical consequence is that the radial couplings between the lowest two wave functions fulfill:

$$\langle\psi_1|\partial/\partial R_1|\psi_2\rangle = \pm\mathcal{P}_{(R_1\leftrightarrow R_2)}\langle\psi_1|\partial/\partial R_2|\psi_2\rangle \qquad (17)$$

where $\mathcal{P}_{(R_1\leftrightarrow R_2)}$ is the mirror image operator, and the + sign holds for $\alpha < \pi/3$ and the − sign for $\alpha > \pi/3$. Thus, we can obtain from Figs. 9a,b,c the other radial coupling $\langle\psi_1|\partial/\partial R_2|\psi_2\rangle$ by taking in Figs. 9a,b the mirror image of $\langle\psi_1|\partial/\partial R_1|\psi_2\rangle$, obtained by interchanging $R_1 \leftrightarrow R_2$, while in Fig. 9c for $\alpha > \pi/3$ we must take the opposite of the mirror image. We thus have a discontinuity of both couplings at the $\alpha = \pi/3$ plane.

C. Electronic structure in terms of Jacobi coordinates.

It is interesting, and useful, to consider the corresponding situation when using Jacobian coordinates, which we now present in a condensed form, using the contour in Fig. 13. The (arrow) *loci* of Fig. 12 only appear for $\rho = R_0$ and R large, and the conical seam for $\rho = 2R/\sqrt{3}$, $\theta = \pi/2$. Starting from $\theta < \pi/2$, the initial steps (reference points 1 to 3) are identical to those of Fig. 12; step 4 is intermediate to the previous situation between 3 and 4, and the wave functions in step 5 (for $\theta = \pi/2$) are the same as the previous 4. Hence, along the lowest part of the loop we have two sign reversals. The upper half of the cycle for $\theta > \pi/2$ (points 10 to 7) is the same as the first half (points 1 to 4), by interchanging $s_a \leftrightarrow s_b$, and we then have two sign reversals too. We finally have an extra sign reversal as θ crosses $\pi/2$ (point 5). This makes up a total of five sign changes, hence an overall sign reversal for ψ_2 when going around the full cycle. As before, we can also choose to go around the smaller 2 - 5 - 8 loop, with three sign changes. The overall situation is, as expected, similar as for the bond coordinates.

The practical consequences differ, however, since it is clear that one can now choose the radial couplings $\partial/\partial\rho$ and $\partial/\partial R$ to be the same for θ and $\pi - \theta$, so that if one neglects Coriolis couplings the topological phase yields no difficulties with Jacobi coordinates! Of course there must be a snag, and this is that these couplings are large in a wide domain of the $\{\rho, R\}$ plane, for angles close to $\pi/2$, as we have checked. Indeed, if one neglects the small $\partial/\partial\alpha$ coupling to simplify the algebra, we readily obtain for θ close to $\pi/2$:

$$\langle\psi_1|\partial/\partial\theta|\psi_2\rangle = \pm\frac{\rho R}{2\sqrt{R^2+\rho^2/4}}|\langle\psi_1|\partial/\partial R_2|\psi_2\rangle| \quad (18)$$

where the + sign holds for $\theta > \pi/2$ and the − sign for $\theta < \pi/2$. Clearly, these matrix elements give rise to large Coriolis couplings. Then, if one incorporates these couplings in the dynamics, one finds that they are discontinuous across the $\theta = \pi/2$ plane. Another possibility is to take them to be continuous across the $\theta = \pi/2$ plane, by taking the sign of ψ_2 to be opposite in the reference points 6 to 9 of table I. However, then the $\partial/\partial\rho$ and $\partial/\partial R$ interactions have opposite signs for θ and $\pi - \theta$, with the same consequences as for the bond coordinates.

D. Accuracy of the DIM data. Some elementary Quantum Chemistry.

Since the previous reasoning is based on valence-bond (i.e., DIM type) wave functions, we now turn to the question of how well the molecular data are reproduced by the DIM method near the conical seam between the second and third PESs. To illustrate our findings on this point, we first show in Figs. 15a,b the lowest molecular energies obtained with the DIM and *ab initio* methods for $\alpha = \pi/4$ and $R_1 = 2$ and 3 a_0, as functions of R_2. These figures illustrate the fact that for $R_1 > 2.5$ both sets of energies for the lowest two PESs are close. On the other hand, for $R_1 < 2.4$, several *ab initio* curves are inserted between the second and third DIM ones. In particular, the conical seam between the second and third PES is replaced by an apparently different one at the same location ($R_1 = R_2 = R_3$). To explain these findings, and in the same spirit as in the previous section, we use some qualitative arguments from elementary Quantum Chemistry.

Along the seam, the standard DIM method employs valence-bond configurations whose un-normalized spatial parts have the forms:

$$\begin{aligned}
\psi_1 &= (s_a s_b + s_b s_c + s_c s_a) + (s_b s_a + s_c s_b + s_a s_c) \\
\psi_2 &= (s_a - s_b)s_c + s_c(s_a - s_b) \\
\psi_3 &= (s_a s_c + s_b s_c - 2s_a s_b) \\
&\quad +(s_c s_a + s_c s_b - 2s_b s_a)
\end{aligned} \quad (19)$$

where ψ_1 has A_1' symmetry, while ψ_2 and ψ_3 transform like the two-dimensional E′ representation of D_{3h} so that any linear combination of them will also do.

We now turn to the corresponding *ab initio* wave functions and, as before, we consider the dominant contributions at the $R_1 = R_2 = R_3$ seam. These are constructed from the self-consistent-field molecular orbitals whose dominant form is:

$$\begin{aligned}
\varphi_1 &= s_a + s_b + s_c \\
\varphi_2 &= s_a - s_b \\
\varphi_3 &= s_a + s_b - 2s_c
\end{aligned} \quad (20)$$

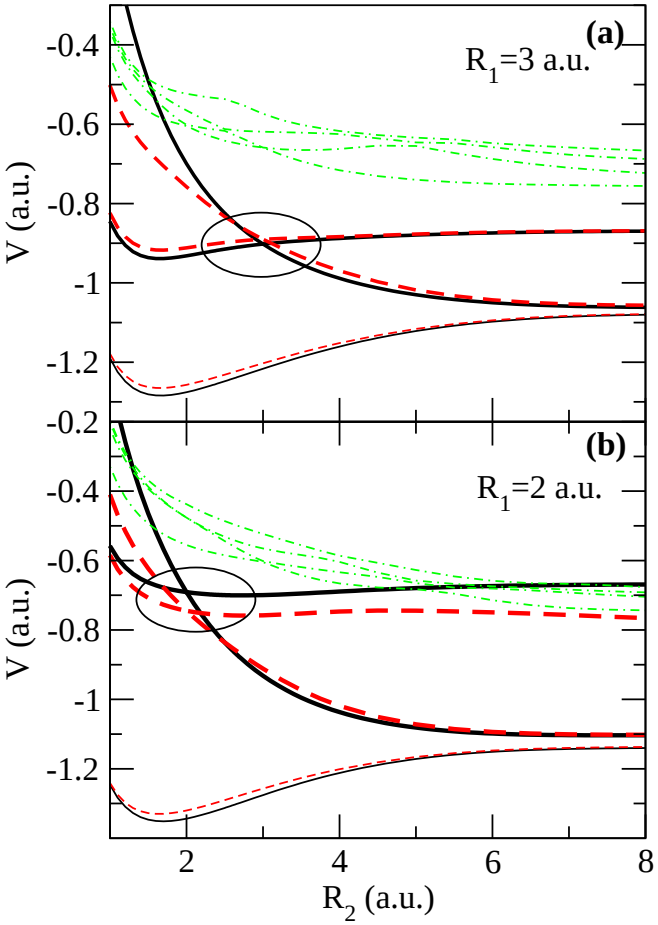

FIG. 15: Comparison between *ab initio* (solid and dashed-dotted lines) and DIM (broken lines) potential energy curves for $\alpha = 60°$ as function of R_2 for two values of R_1 (indicated in the panels). An ellipse marks the conical intersection between the second and third state.

of A_1' and E′ symmetry, respectively. The corresponding dominant configurations are:

$$\begin{aligned}
\Psi_1 &= (s_a + s_b + s_c)^2 \\
\Psi_2 &= (s_a - s_b)(s_a + s_b + s_c) + (s_a + s_b + s_c)(s_a - s_b) \\
\Psi_3 &= (s_a + s_b - 2s_c)(s_a + s_b + s_c) \\
&\quad +(s_a + s_b + s_c)(s_a + s_b - 2s_c)
\end{aligned} \quad (21)$$

It is straightforward to see that the covalent part of these wave functions coincide with their DIM counterparts. We conclude that provided that in the corresponding configuration interaction wave functions the ionical parts as well as three-body effects have negligible weights, the DIM and corresponding *ab initio* data will be very close. For a wide domain of nuclear configurations near the conical seam, this is indeed the case, and Fig. 15a provides an example of this situation. On the other hand, the former approximation does not hold for the *third* state far from the conical seam, as for $R_2 \to \infty$, when the bond distance $R_1 < 2.4$ since then the energy of the excited $H_2(^1\Sigma_u^+)$ state lies lower than that of $H_2^+(\sigma_u)$+H(1s). In

this unfavorable case, the asymptotic form of the *ab initio* functions are:

$$\begin{aligned}\Psi_1 &= (s_a + s_b)^2 \\ \Psi_2 &= s_c(s_a + s_b) + (s_a + s_b)s_c \\ \Psi_3 &= (s_a - s_b)(s_a + s_b) + (s_a + s_b)(s_a - s_b) \quad (22)\end{aligned}$$

representing $H_2(^1\Sigma_g^+)$+H^+, $H_2^+(\sigma_g)$+H(1s) and $H_2(^1\Sigma_u^+)$+H^+, respectively, while the DIM counterparts cannot describe the ionic state Ψ_3 and we obtain:

$$\begin{aligned}\psi_1 &= s_a s_b + s_b s_a \\ \psi_2 &= s_c(s_a + s_b) + (s_a + s_b)s_c \\ \psi_3 &= s_c(s_a - s_b) + (s_a - s_b)s_c \quad (23)\end{aligned}$$

representing $H_2(^1\Sigma_g^+)$+H^+, $H_2^+(\sigma_g)$+H(1s) and $H_2^+(\sigma_u)$+H(1s), respectively. This incorrect limiting behavior then results in an inaccurate asymptotic value for the third PES at large R_2 values. The situation is improved when R_2 diminishes, as the bonding orbital in Eq. (22) takes up an s_c component, so that when R_2 reaches a value close to R_0 this orbital is roughly of the form φ_1 in Eq. (20). Accordingly, as R_2 diminishes, we have that Ψ_3 takes up a covalent component, and when the conical seam is reached, it approximately has the structure of Eq. (21), whose covalent part is of the form of ψ_3 in (19). Therefore, we conclude that even in the unfavorable case the conical seams between the *ab initio* and DIM second and third PES are "the same". However, in that case, although the asymptotic error of the third DIM PES diminishes at small R_2 values, it is not negligible, and the approximation afforded by the DIM method near the seam is less accurate. An example of this situation is shown in Fig. 15b. Notwithstanding this case, we conclude that the agreement between our new DIM and *ab initio* data is, for practical purposes, much better than surmised in I: not only the geometrical phase problem appears in the same way and at the same nuclear configurations, but even the overall quantitative behavior of the DIM results near the conical seam is appropriate, so that we can only expect inaccuracies to arise in the dynamics when transitions to the third state are crucial in the limited domains of nuclear configurations just considered in Fig. 15

IV. SUMMARY AND CONCLUSIONS.

The H_3^+ system is simple in the sense that it has only two electrons, but not in any other sense. Even restricting our attention to the ground electronic state, its complications become apparent as soon as one considers the asymptotic domains of large nuclear distances, where there appear three conical seams between the ground and first excited PES. A study of these domains has been the main subject matter of the present work, thus complementing a previous treatment, reported in I. We have described two main features of the wave functions and non-adiabatic couplings that must be taken into account in any close-coupling calculation of inelastic (whether vibrational or electronic) collisions of the H^++H_2, H_2^+ + H reactions and isotopical counterparts. These are: that one must implement a non-standard treatment of the quasi-singular interactions appearing near the conical seams, as well as a way to deal with discontinuities in the remaining coupling surfaces there and elsewhere. We have stressed that singularities and discontinuities pose different and important technical difficulties in the setting up of a proper interpolation scheme of the molecular data.

In Sec. II we have proposed, and employed, a way to deal with the first feature. The procedure consists in a local diabatization of the couplings, and requires a large amount of these data, as well as a non-decreasing accuracy when such large internuclear distances are reached that the singular behavior is apparent. For this purpose, we have taken into account that in those asymptotic regions three-body interactions are small; accordingly, a DIM calculation that uses as input the diatomic energies obtained from the same *ab initio* program and basis set as for the triatomic yields very close results to this latter. Because of its computational efficiently and flexibility, the former method can then be employed to calculate a large enough amount of data to parameterize an exponential-linear model, as done in Sec. II; the resulting expressions can then be interpreted also as a fit to the *ab initio* data. Hence, one can then employ either the DIM or *ab initio* molecular data, as needed, to describe the domain of smaller internuclear distances; see Fig. 5 for the connecting region. It has the small inconvenience, however, that our fit of the DIM data is only accurate for the particular *ab initio* results obtained with our basis set: use of other *ab initio* data would require a (slightly) different parameters. Hence, what we present is a *modus operandi*, rather than a specific parameterization for general use, such as those of Refs. [30–33] for the energy of the ground PES. Once the PESs and couplings are parameterized, we perform a local diabatization procedure that eliminates the singularities of the dynamical couplings, as illustrated in Figs. 7 and 8. Our aim is thus more modest than in I, where a diabatization of the entire surface was attempted; this had the undesirable result that residual couplings obtained from *ab initio* calculations turned out to be sizeable.

The second feature is due to the existence of a fourth conical seam, this time between the second and third PES, that lies in the equilateral nuclear configuration, and which makes the gradient of the second PES discontinuous. More importantly, it also gives rise to a discontinuity of the couplings between the first two states at the $\alpha = \pi/3$ plane in Fig. 12 and $\theta = \pi/2$ plane in Fig. 13, because a phase change is introduced when the nuclear geometry changes in such a way as to describe a closed loop in nuclear configuration space enclosing the extra intersection.

By modifying the pioneer explanation of Herzberg and Longuet-Higgins to include resonance rather than exchange forces, we have presented in section III, in a compact way, the qualitative evolution of the wave functions and couplings in both bond and Jacobi parameter spaces. In this way the three conical regions are connected, and we have thus seen how the phase change arises for both *ab initio* and DIM calculations when the bond angle α crosses values of $\pi/3$. We have discussed the accuracy of the DIM approach, which (as modified here) is better than surmised in our previous article.

We have also pointed out the curious feature that the discontinuity in the couplings is formally avoided when using Jacobi coordinates, and neglecting rotational, or Coriolis, couplings, as shown in Sec. III C. However, we also pointed out there that these couplings are large, and discontinuous when the angle θ approaches values of $\pi/2$. Furthermore, if one wishes to obtain them, it seems more convenient to employ the molecular data in terms of bond coordinates (R_1, R_2, α in Sec. II), possibly neglecting $\langle\psi_1|\partial/\partial\alpha|\psi_2\rangle$, and then obtaining the matrix elements $\langle\psi_1|\partial/\partial\rho|\psi_2\rangle$, $\langle\psi_1|\partial/\partial R|\psi_2\rangle$, $\langle\psi_1|\partial/\partial\theta|\psi_2\rangle$ from $\langle\psi_1|\partial/\partial R_1|\psi_2\rangle$ and $\langle\psi_1|\partial/\partial R_2|\psi_2\rangle$. We note that the Coriolis couplings are neglected in infinite order sudden approximation (IOSA and RIOSA) and trajectory surface hopping methods (TSH), and it would be interesting to know the consequences of this approximation. We finally mention that no difficulties due to the discontinuous couplings are encountered at high impact energies when using semi-classical approaches with rectilinear nuclear trajectories [34–36], or with methods that do not employ adiabatic wave-functions [37].

ACKNOWLEDGMENTS

This work has been partially supported by MEC projects FIS2004-04145 and ENE2004-06266, and by the program PR2005-0004. IR acknowledges MEC for a "Ramón y Cajal" contract. AR acknowledges the contract PR2005-0004 and useful discussions with the research group at the Department of Physical Chemistry, University of Barcelona.

[1] P. Barragán, L. F. Errea, L. Méndez, A. Macías, I. Rabadán, A. Riera, J. Lucas, and A. Aguilar, J. Chem. Phys. **121**, 11629 (2004).
[2] C. W. B. Jr., S. V. O'Neil, R. K. Preston, H. F. S. III, and C. F. Bender, J. Chem. Phys. **59**, 1286 (1973).
[3] J. R. Krenos, R. K. Preston, R. Wolfgang, and J. C. Tully, J. Chem. Phys. **60**, 1674 (1974).
[4] M. Chajia and R. Levine, Phys. Chem. Chem. Phys. **1**, 1205 (1999).
[5] R. B. Gerber, Chem. Phys. **16**, 19 (1976).
[6] M. Baer, G. Niedner-Schatteburg, and J. P. Toennies, J. Chem. Phys. **91**, 4169 (1989).
[7] G. Herzberg and H. C. Longuet-Higgins, Discuss. Far. Soc. **35**, 77 (1963).
[8] M. V. Berry, Proc. Roy. Soc. **392**, 45 (1984).
[9] H. C. Longuet-Higgins, Proc. Roy. Soc. **344**, 147 (1975).
[10] A. M. Mebel, G. J. Halász, A. Vibók, A. Alijah, and M. Baer, J. Chem. Phys. **117**, 991 (2002).
[11] S. Han and D. R. Yarkony, J. Chem. Phys. **119**, 5058 (2003).
[12] R. Englman, A. Yahalom, M. Baer, and A. M. Mebel, Int. J. Quant. Chem. **92**, 135 (2003).
[13] G. Halász, A. Vibók, A. M. Mebel, and M. Baer, J. Chem. Phys. **118**, 3052 (2003).
[14] A. Vibók, G. Halász, and M. Baer, Chem. Phys. Lett. **399**, 7 (2004).
[15] T. Vértesi, A. Vibók, G. Halász, and M. Baer, J. Phys. B: At. Mol. Opt. Phys. **37**, 4603 (2004).
[16] M. Baer, Chem. Phys. Lett. **329**, 450 (2000).
[17] M. Baer, J. Phys. Chem. A **105**, 2198 (2001).
[18] E. R. Davidson, in *MOTECC, Modern Techniques in Computational Chemistry*, edited by E. Clementi (ESCOM Publishers B. V., Leiden, 1990).
[19] P. O. Widmark, P. Malmqvist, and B. Roos, Theor. Chim. Acta **77**, 291 (1990).
[20] J. F. Castillo, L. F. Errea, A. Macías, L. Méndez, and A. Riera, J. Chem. Phys. **103**, 2113 (1995).
[21] L. F. Errea, L. Fernández, A. Macías, L. Méndez, I. Rabadán, and A. Riera, J. Chem. Phys. **121**, 1663 (2004).
[22] L. F. Errea, L. Fernández, L. Méndez, A. Macías, I. Rabadán, and A. Riera, Phys. Rev. A **69**, 012705 (2004).
[23] L. F. Errea, A. Macías, L. Méndez, B. Pons, and A. Riera, J. Chem. Phys. **118**, 325 (2003).
[24] F. O. Ellison, J. Am. Chem. Soc. **85**, 3540 (1963).
[25] L. D. Landau, Pys. Z. Sowetjetunion **2**, 46 (1932).
[26] C. Zener, Proc. R. Soc. London **Ser. A 137**, 696 (1932).
[27] D. R. Yarkony, Rev. Mod. Phys. **68**, 985 (1996).
[28] Z. Xu, M. Baer, and A. J. C. Varandas, J. Chem. Phys. **112**, 2746 (2000).
[29] A. Riera, J. Mol. Spec. **300**, 93 (1993).
[30] C. F. Giese and W. R. Gentry, Phys. Rev. A **10**, 2156 (1974).
[31] A. Aguado, O. Roncero, C. Tablero, C. Sanz, and M. Paniagua, J. Chem. Phys. **112**, 1240 (2000).
[32] R. Prosmiti, O. L. Polyansky, and J. Tennyson, Chem. Phys. Lett. **273**, 107 (1997).
[33] O. L. Polyansky, R. Prosmiti, W. Klopper, and J. Tennyson, Mol. Phys. **98**, 261 (2000).
[34] D. Elizaga, L. F. Errea, A. Macías, L. Méndez, A. Riera, and A. Rojas, J. Phys. B: At. Mol. Opt. Phys. **32**, L697 (1999).
[35] L. F. Errea, A. Macías, L. Méndez, I. Rabadán, A. Riera, A. Rojas, and P. Sanz, Phys. Rev. A **63**, 062713 (2001).
[36] T. Kusakabe, L. Pichi, R. J.Buenker, M. Kimura, and H. Tawara, Phys. Rev. A **70**, 052710 (2004).
[37] J. Morales, A. Diz, E. Deumens, and Y. Öhrn, J. Chem. Phys. **103**, 9968 (1995).